

Automated femur segmentation from computed tomography images using a deep neural network

P.A. Bjornsson^{*a}, B. Helgason^b, H. Palsson^c, S. Sigurdsson^d, V. Gudnason^{d,e}, and L.M. Ellingsen^{a,f}

^aDept. of Electrical and Computer Engineering, The University of Iceland, Reykjavik, Iceland

^bInstitute for Biomechanics, ETH Zürich, Zürich, Switzerland

^cDept. of Industrial Engineering, Mechanical Engineering, and Computer Science, The University of Iceland, Reykjavik, Iceland

^dThe Icelandic Heart Association, Kopavogur, Iceland

^eDept. of Medicine, The University of Iceland, Reykjavik, Iceland

^fDept. of Electrical and Computer Engineering, The Johns Hopkins University, Baltimore, MD 21218, USA

ABSTRACT

Osteoporosis is a common bone disease that occurs when the creation of new bone does not keep up with the loss of old bone, resulting in increased fracture risk. Adults over the age of 50 are especially at risk and see their quality of life diminished because of limited mobility, which can lead to isolation and depression. We are developing a robust screening method capable of identifying individuals predisposed to hip fracture to address this clinical challenge. The method uses finite element analysis and relies on segmented computed tomography (CT) images of the hip. Presently, the segmentation of the proximal femur requires manual input, which is a tedious task, prone to human error, and severely limits the practicality of the method in a clinical context. Here we present a novel approach for segmenting the proximal femur that uses a deep convolutional neural network to produce accurate, automated, robust, and fast segmentations of the femur from CT scans. The network architecture is based on the renowned u-net, which consists of a downsampling path to extract increasingly complex features of the input patch and an upsampling path to convert the acquired low resolution image into a high resolution one. Skipped connections allow us to recover critical spatial information lost during downsampling. The model was trained on 30 manually segmented CT images and was evaluated on 200 ground truth manual segmentations. Our method delivers a mean Dice similarity coefficient (DSC) and 95th percentile Hausdorff distance (HD95) of 0.990 and 0.981 mm, respectively.

Keywords: Computed tomography, Femur, Segmentation, Convolutional neural networks, Osteoporosis.

1. INTRODUCTION

A consequence of ageing societies is a higher prevalence of chronic diseases amongst older populations. In the coming years, this will lead to shortages of qualified health care practitioners and mounting health care costs as a result of the added strain placed by these longevous populations. It appears that the current status quo of health care systems is unsustainable and must be restructured from face-to-face based care to a more decentralized, home based care that places emphasis on prevention rather than treatment. One disease that disproportionately affects those over the age of 50 is osteoporosis - a bone disease that occurs when the body loses too much bone, makes too little bone, or both, resulting in reduced bone mass, which leads to increased bone fragility and heightened fracture risk with age. Hip fractures are associated with some of the most dire socioeconomic consequences: those who incur a fracture typically experience a steep decline in physical, mental, and emotional function and, in 50-55% of cases, individuals are left with residual walking disability and in 15-30% of cases,

Further author information: (Send correspondence to P.A.B.)

P.A.B.: E-mail: pab11@hi.is

L.M.E.: E-mail: lotta@hi.is

these individuals must be remanded to institutional care.¹⁻⁵ What is most startling is that 11-23% of individuals will be deceased six months after incurring the fracture, increasing to 22-29% after one year has passed since the incident.⁶

Subject-specific, image-based finite element (FE) analysis of bone is a popular approach in biomechanics that has gained considerable traction in recent years.⁷ By exploiting the gray-scale features of the CT images in concert with the respective segmentation mask, a screening tool for hip fracture risk prediction can be brought to fruition. Such a clinical screening tool could prevent potentially devastating fractures for patients, as well as to dramatically relieve the economic burden of hip fractures on our healthcare systems. However, these methods have yet to be implemented for clinical use, since the segmentation of the proximal femur currently requires manual input, which severely limits their use in clinical context.

A number of methods have been implemented to surmount the problem of bone segmentation, ranging from thresholding techniques to graph-cut methods.⁸⁻¹¹ Current segmentation methods often require a “user-in-the-loop” paradigm in order to manually correct segmentations to produce acceptable masks for FE modeling and/or their processing time is too long for clinical use. This lack of robustness is costly in terms of time and the need for a highly trained specialist to manually correct the segmentations. Consequently, these methods cannot process larger cohorts to the same degree as fully automated ones. In recent years, the application of deep neural networks (DNNs) in image segmentation has gained considerable attention. The use of deep neural networks as a viable option for biomedical image segmentation is a direct consequence of the u-net architecture proposed by Ronneberger et al.¹² In this impactful paper, they demonstrated how the u-net architecture can produce fast and precise segmentations without relying on a large training set. However, the process by which ground truth segmentation masks are authored is typically manual delineation, which is a taxing and time-consuming process that is ideally only implemented for a small training data set. Despite the need for ground truth labels, deep neural networks have become the state-of-the-art approach in medical imaging.^{13,14} A segmentation prediction on novel data can be generated autonomously (i.e., without human intervention) in a matter of seconds, which is often an order of magnitude faster than preceding methods that do not make use of DNN’s. Zhao et al.¹⁵ proposed an automated, patch-based three-dimensional v-net architecture¹⁶ and reported a mean DSC of 0.9815 ± 0.0009 . Another successful method based on the u-net architecture¹² was conducted by Chen et al.,¹⁷ who reported a mean DSC of 0.9688 ± 0.0095 . The major drawback to these two methods, however, is their dependence on large training sets that require ground truth segmentations, as well as the small validation sets they have been evaluated on. The arduous nature of authoring these ground truth segmentations, as previously mentioned, is oftentimes not feasible and severely limits the practicality of these methods.

Here we propose a fully automated method for segmenting the proximal femur from CT scans that is accurate, robust, and faster than other state-of-the-art methods. We evaluate our method on 200 manually delineated ground truth annotations from the Age, Gene/Environment Susceptibility-Reykjavik Study (AGES-RS),¹⁸ a unique longitudinal study of the Icelandic elderly, to demonstrate the accuracy and robustness of our proposed method.

2. METHODS

2.1 Preprocessing and data augmentation

The Icelandic Heart Association (IHA) provided us with CT images from the AGES-RS:¹⁸ a cohort that consists of both men and women born between 1907 and 1935, monitored in Iceland by the IHA since 1967. This unique database of high-quality CT images contains roughly 4800 density calibrated CT scans of the proximal femur at baseline and 3300 scans of the same individuals acquired at a five-year follow-up. The in-plane resolution of each scan is 512×512 voxels with 88-178 slices and $0.977 \times 0.977 \times 1$ mm³ voxel size. The preprocessing of the data consisted of three steps: Firstly, each of the 30 CT images used for training was split in half and the left sides were subsequently mirrored to the right, resulting in 60 images of the right side hip/upper leg. Second, min-max normalization was used to linearly map the intensity values from Hounsfield units to the range $[0, 1]$. Lastly, Otsu thresholding¹⁹ was implemented to identify the background voxels and allow for automatic cropping of the 3D images to decrease their size and therefore speed up the execution of the neural network. Since each extra voxel is computationally costly, the images were all cropped to eliminate unnecessary background voxels.

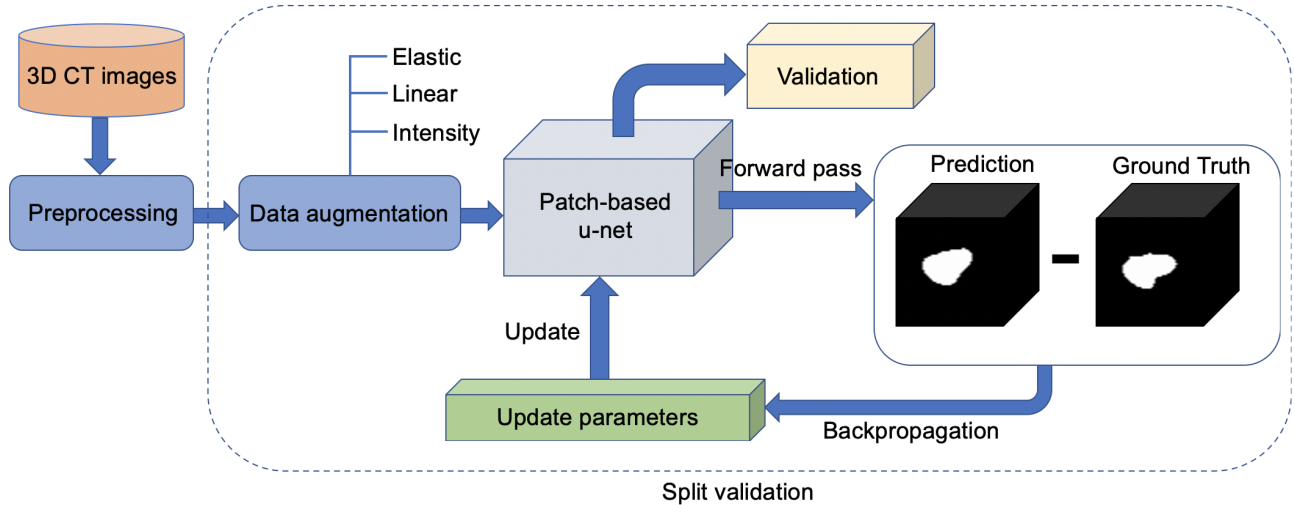


Figure 1. A flowchart showing the workflow of our proposed method.

The proposed fully automated proximal femur segmentation pipeline is illustrated in Figure 1. During training, a training/validation set of 30 CT images (i.e., 60 proximal femurs) from the AGES cohort¹⁸ was fed into a neural network that exploited on-the-fly data augmentation on randomly cropped patches from a randomly selected batch of two images. On-the-fly data augmentation eliminates the need for excessive storage of augmented images by performing the augmentation prior to each optimization iteration. Data augmentation is imperative for maximizing the efficiency of a training set, since obtaining manual segmentations (i.e., ground truth segmentations) is an arduous, time-consuming process that does not cater to large cohorts. Hence, data augmentation is applied to teach the model invariance and robustness properties when only a limited data set is available. In addition, artificially expanding the training set with data augmentation has a regularizing effect, which avoids overfitting the model to a small subset of data. Deformations that capture variation within the data set can be simulated efficiently and assist the model in learning invariance between images.¹² Here we applied elastic deformations as well as linear-spatial and intensity transformations (i.e., scaling, rotation and brightness) to simulate the variability between patients’ scans. Data augmentation, with random transformation parameters from pre-defined ranges, was implemented on-the-fly for each image before it was forwarded into the neural network. Each transformation had a 35% likelihood of being applied to the image at hand, allowing the model to encounter a diverse set of images, thereby decreasing redundancy. The scaling, rotation, and brightness transforms were defined in the ranges $(0.95, 1.05)$, $(-3^\circ, 3^\circ)$, and $(0.75, 1.25)$, respectively, while the elastic deformation transform was tuned to $\alpha = (0, 100)$ and $\sigma = (9, 13)$.^{*} On-the-fly data augmentation, in concert with parameter sharing²⁰ and batch normalization,²¹ rendered the use of explicit regularization techniques unnecessary and even counterproductive.

2.2 The segmentation workflow and model architecture

As previously stated, the u-net architecture addresses two main issues: namely, the ability to train a model from a very small data set and the ability to produce precise segmentations despite the former. A schematic of the proposed architecture is shown in Figure 2. The two paths that comprise the u-net structure are the contracting (downsampling) path and the expanding (upsampling) path. The former is the encoder and captures context with the use of stacked convolutional units and max pooling layers, while the latter is the decoder and allows for precise localization with the use of transposed convolutions. In the final layer of the network, a $1 \times 1 \times 1$ convolution is used to map the feature map to the number of classes. By applying a softmax layer voxel-wise, a probabilistic map is outputted that gives each voxel a value in the range $[0, 1]$; voxels with a probability > 0.5 belong to the foreground class (proximal femur) and the rest to the background class. The proposed method was implemented using the MIScnn framework²² in Python.

^{*}Here, α denotes the scaling factor (controls the deformation intensity) and σ denotes the smoothing factor (controls the displacement field smoothing) for the elastic deformation.

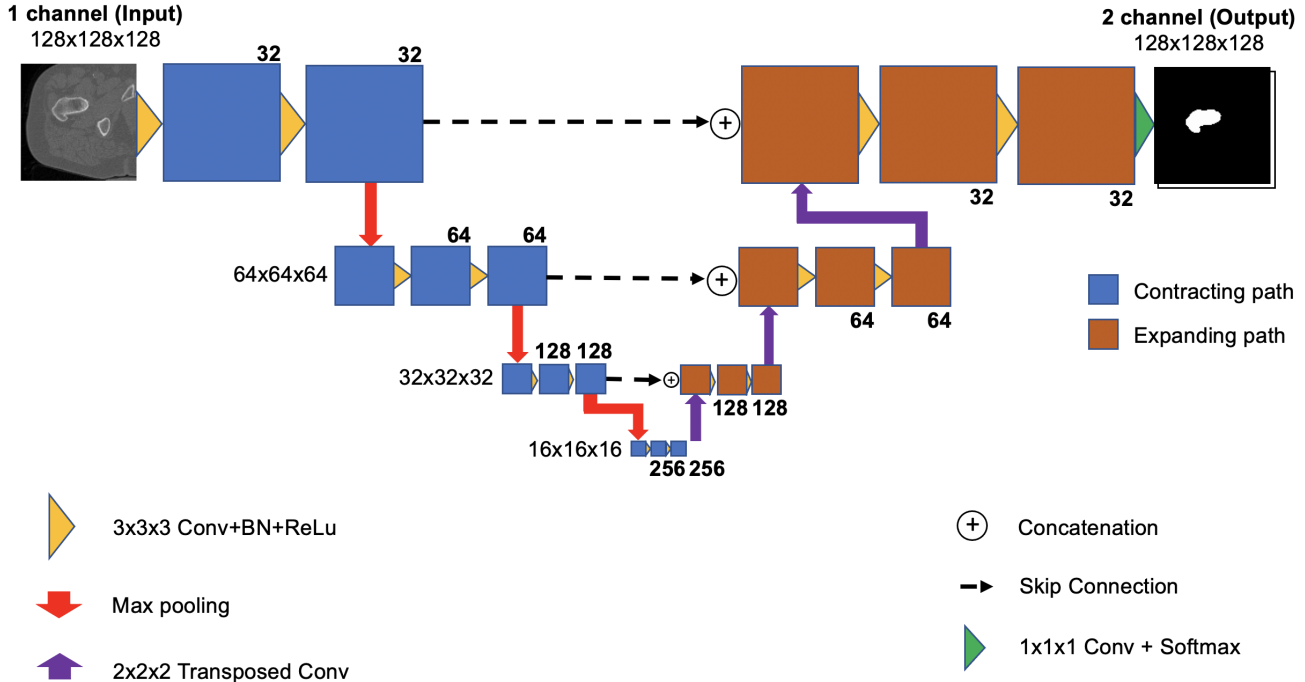


Figure 2. A schematic of our proposed 3D u-net model. The bold numbers at the corners represent the number of feature maps (channels) per layer. For the sake of simplicity, feature maps are depicted in two dimensions.

A patch-based model was adopted in consideration of memory constraints; each volume patch was $128 \times 128 \times 128$ voxels with an overlap of $64 \times 64 \times 64$ voxels. This patch size captures the entire femoral head, which is the most dynamic section of the proximal femur, and downsamples nicely, meaning that after each use of max pooling we are left with integer values for patch dimensions. During training, volume patches were randomly selected from the image volume and subsequently fed into the neural network. As the image patch is downsampled in the contracting path, the number of channels increases, which allows for the extraction of more complex features. Skip connections are used to pass features from the contracting path to the expanding path in order to recover spatial information lost during downsampling. At each step in the decoder, a skip connection allows for the concatenation of the output of the transposed convolutional layer with the corresponding feature map from the encoder. A convolutional layer is subsequently able to produce a more precise output based on this information. The Dice loss function, defined as $1 - \text{DSC}$, quantified the performance of the model at each iteration of each epoch in order for the gradient descent algorithm to adjust the parameters during backpropagation. The validation set allowed us to gain insight into the performance of the model on unseen data so that hyperparameters could be adjusted accordingly.

Our model was trained on images from the AGES data set, comprising 260 proximal femurs with corresponding manually delineated segmentations, generated with a semi-automated delineation protocol, that served as ground truth annotations. A total of 54 images were used for training, 6 were used for validation, and the remaining 200 were used for evaluation. The Adam optimizer ($\beta_1 = 0.9$ and $\beta_2 = 0.999$) was used to update the weights with an initial learning rate of $1 \cdot 10^{-4}$. Our model was trained using dual Nvidia GeForce GTX 1080 Ti GPUs for 300 epochs, which took roughly 11.5 hours.

3. EXPERIMENTS AND RESULTS

We evaluated the performance of our model on the aforementioned AGES data set by processing 200 proximal femurs that had been manually segmented (the current gold standard). We used the DSC and HD95 to evaluate the accuracy and robustness of our method. The former metric measures the overlap between the automatically generated segmentation mask and the ground truth manual mask. The HD95 metric, on the other hand, quantifies the largest segmentation error between two images and provides valuable insight into the performance of the

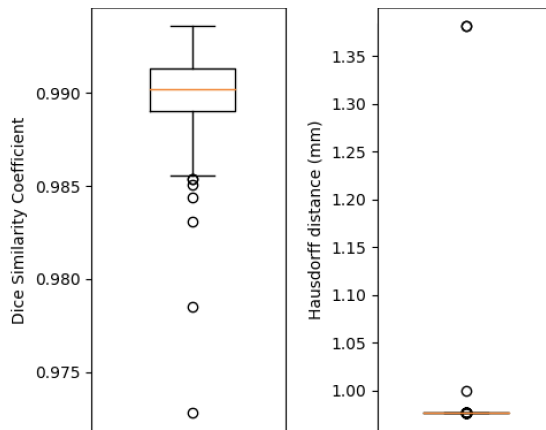


Figure 3. The box plots above show the mean DSC (left) and the mean HD95 (right) for 200 proximal femurs.

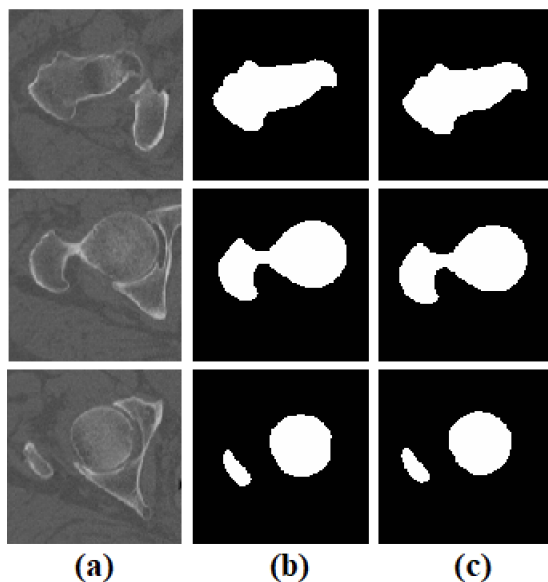


Figure 4. A visual comparison of our segmentation results and the manual segmentation. (a) The original CT scans, (b) the segmentation predictions using the proposed method, (c) the ground truth segmentations.

model. The mean DSC on this evaluation set was 0.990 ± 0.002 and the mean HD95 was 0.981 ± 0.040 mm (see Fig. 3), demonstrating both high accuracy and robustness of the proposed method. The time for each segmentation prediction was 12-15 seconds, making the method viable for use in both large studies and clinical settings. Figure 4 displays a visual comparison between the output of our proposed method and the ground truth segmentation. Despite the thin and diffusive bone structure boundaries between the femoral head and the acetabulum (i.e., the bottom two rows of Figure 4), our method accurately labels the voxels that belong to the foreground class.

4. DISCUSSION AND CONCLUSION

This paper introduces a fully automated, accurate, fast, and robust method for proximal femur segmentation that produces segmentation results with sub-millimeter accuracy. Our model addresses the biggest hurdles that have impeded prior methods. Firstly, it is fully automated and does not require a trained operator to make ad hoc corrections to unacceptable segmentation predictions. Secondly, the time our model takes to output a segmentation prediction (around 12-15 seconds per prediction) is well within reasonable bounds for clinical

viability and can additionally be implemented to process large cohorts. The mean DSC was 0.990 ± 0.002 and mean HD95 was 0.981 ± 0.040 mm when evaluated on 200 manually segmented femurs. The proposed method is superior to preceding methods in terms of previously reported numbers of DSC and HD95 metrics and does not require any manual interaction. In the near future, we will conduct a more extensive evaluation on a larger cohort and, in turn, integrate the method into our existing FE pipeline, bringing it one step closer to becoming a clinically viable option for screening at-risk patients for hip fracture susceptibility.

5. ACKNOWLEDGEMENTS

This work was supported by the RANNIS Icelandic Student Innovation Fund.

REFERENCES

- [1] Ekström, W., Miedel, R., Ponzer, S., Hedström, M., Samnegård, E., and Tidermark, J., “Quality of life after a stable trochanteric fracture—a prospective cohort study on 148 patients,” *J Orthop Trauma* **23**(1), 39–44 (2009).
- [2] Carpenter, R. and Carter, D., “The mechanobiological effects of periosteal surface loads,” *Biomech Model Mechanobiol.* **7**(3), 227–242 (2008).
- [3] Magaziner, J., Fredman, L., Hawkes, W., Hebel, J., Zimmerman, S., Orwig, D., and Wehren, L., “Changes in functional status attributable to hip fracture: A comparison of hip fracture patients to community-dwelling aged,” *Am. J. Epidemiol.* **157**(11), 1023–1031 (2003).
- [4] Nevalainen, T., Hiltunen, L., and Jalovaara, P., “Functional ability after hip fracture among patients home-dwelling at the time of fracture,” *Cent Eur J Public Health* **12**(4), 211–216 (2004).
- [5] Osnes, E., Lofthus, C., Meyer, H., Falch, J., Nordsletten, L., Cappelen, I., and Kristiansen, I., “Consequences of hip fracture on activities of daily life and residential needs,” *Osteoporos Int.* **15**(7), 567–574 (2004).
- [6] Haleem, S., Lutchman, L., Mayahi, R., Grice, J., and Parker, M., “Mortality following hip fracture: Trends and geographical variations over the last 40 years,” *Injury* **39**(10), 1157–1163 (2008).
- [7] Fleps, I., Guy, P., Ferguson, S., Crompton, P., and Helgason, B., “Explicit finite element models accurately predict subject-specific and velocity-dependent kinetics of sideways fall impact,” *J Bone Miner Res.* **34**(10), 1837–1850 (2019).
- [8] Kim, J., Nam, J., and Jang, I., “Fully automated segmentation of a hip joint using the patient-specific optimal thresholding and watershed algorithm,” *Comput Methods Programs Biomed.* **154**, 161–171 (2018).
- [9] Chang, Y., Yuan, Y., Guo, C., Wang, Y., Cheng, Y., and Tamura, S., “Accurate pelvis and femur segmentation in hip ct with a novel patch-based refinement,” *IEEE J Biomed Health Inform.* **23**(3), 1192–1204 (2020).
- [10] Younes, L., Nakajima, Y., and Saito, T., “Fully automatic segmentation of the femur from 3d-ct images using primitive shape recognition and statistical shape models,” *Int J Comput Assist Radiol Surg.* **9**(2), 189–196 (2019).
- [11] Pauchard, Y., Fitze, T., Browarnik, D., Eskandari, A., Pauchard, I., Enns-Bray, W., Pálsson, H., Sigurdsson, S., Ferguson, S. J., Harris, T. B., Gudnason, V., and Helgason, B., “Interactive graph- cut segmentation for fast creation of finite element models from clinical ct data for hip fracture prediction,” *Comput Methods Biomech Biomed Engin.* **20**(3), 342 (2016).
- [12] Ronneberger, O., Fischer, P., and Brox, T., “U-net: Convolutional networks for biomedical image segmentation,” in *[Medical Image Computing and Computer-Assisted Intervention – MICCAI 2015]*, Navab, N., Hornegger, J., Wells, W. M., and Frangi, A. F., eds., 234–241, Springer International Publishing, Cham (2015).
- [13] Shao, M., Han, S., Carass, A., Li, X., Blitz, A., Shin, J., Prince, J., and Ellingsen, L. M., “Brain ventricle parcellation using a deep neural network: Application to patients with ventriculomegaly,” *NeuroImage: Clinical* **23**, 101871 (2019).
- [14] Huo, Y., Terry, J., Wang, J., Nair, S., Lasko, T., Freedman, B., Carr, J., and Landman, B., “Fully automatic liver attenuation estimation combining cnn segmentation and morphological operations,” *Med. Phys.* **46**(8), 3508–3519 (2019).

- [15] Zhao, C., Keyak, J., Tang, J., Kaneko, T. S., Khosla, S., Amin, S., Atkinson, E., Zhao, L., Serou, M., Zhang, C., Shen, H., Deng, H., and Zhou, W., “A deep learning-based method for automatic segmentation of proximal femur from quantitative computed tomography images,” *ArXiv. abs/2006.05513* (2020).
- [16] Milletari, F., Navab, N., and Ahmadi, S., “V-net: Fully convolutional neural networks for volumetric medical image segmentation,” in [*3DV 2016*], (2016).
- [17] Chen, F., Liu, J., Zhao, Z., Zhu, M., and Liao, H., “Three-dimensional feature-enhanced network for automatic femur segmentation,” *IEEE J Biomed Health Inform.* **23(1)**, 243–252 (2019).
- [18] Harris, T., Launer, L., Eiriksdottir, G., Kjartansson, O., Jonsson, P., Sigurdsson, G., Thorgeirsson, G., Aspelund, T., Garcia, M., Cotch, M., Hoffman, H., and Gudnason, V., “Age, gene/environment susceptibility – reykjavik study: Multidisciplinary applied phenomics,” *Am J Epidemiol.* **165(9)**, 1076–1087 (2007).
- [19] Otsu, N., “A threshold selection method from gray-level histograms,” *IEEE Trans. Syst.* **9(1)**, 62–66 (1979).
- [20] LeCun, Y., Boser, B., Denker, J., Henderson, D., Howard, R., Hubbard, W., and Jackel, L., “Handwritten digit recognition with a back-propagation network,” in [*Advances in Neural Information Processing Systems*], Touretzky, D., ed., **2**, 396–404, Morgan-Kaufmann (1990).
- [21] Ioffe, S. and Szegedy, C., “Batch normalization: Accelerating deep network training by reducing internal covariate shift,” *CoRR* **abs/1502.03167** (2015).
- [22] Müller, D. and Kramer, F., “Miscnn: A framework for medical image segmentation with convolutional neural networks and deep learning,” *ArXiv* **abs/1910.09308** (2019).